Cloud-Base Height Estimation from VIIRS. Part II: A Statistical Algorithm Based on A-Train Satellite Data

YOO-JEONG NOH, JOHN M. FORSYTHE, STEVEN D. MILLER, AND CURTIS J. SEAMAN

Cooperative Institute for Research in the Atmosphere, Colorado State University, Fort Collins, Colorado

YUE LI

Cooperative Institute for Meteorological Satellite Studies, University of Wisconsin–Madison, Madison, Wisconsin

ANDREW K. HEIDINGER

NOAA/NESDIS/Center for Satellite Applications and Research/Advanced Satellite Products Branch, Madison, Wisconsin

DANIEL T. LINDSEY

NOAA/NESDIS/Center for Satellite Applications and Research/Regional and Mesoscale Meteorology Branch, Fort Collins, Colorado

MATTHEW A. ROGERS AND PHILIP T. PARTAIN

Cooperative Institute for Research in the Atmosphere, Colorado State University, Fort Collins, Colorado

ABSTRACT

Knowledge of cloud-base height (CBH) is important to describe cloud radiative feedbacks in numerical models and is of practical relevance to the aviation community. Whereas satellite remote sensing with passive radiometers traditionally has provided a ready means for estimating cloud-top height (CTH) and cloud water path (CWP), assignment of CBH requires heavy assumptions on the distribution of CWP within the cloud profile. An attempt to retrieve CBH has been included as part of the VIIRS environmental data records, produced operationally as part of the *Suomi–National Polar-Orbiting Partnership* (*SNPP*) and the forthcoming Joint Polar Satellite System. Through formal validation studies tied to the program, it was found that the operational CBH algorithm failed to meet performance specifications in many cases. This paper presents a new methodology for retrieving CBH of the uppermost cloud layer, developed through statistical analyses relating cloud geometric thickness (CGT) to CTH and CWP. The semiempirical approach, which relates these parameters via piecewise fitting, enlists A-Train satellite data [*CloudSat* cloud profiling radar (CPR), *CALIPSO/*CALIOP, and *Aqua* MODIS]. CBH is provided as the residual difference between CTH and CGT. By eliminating cloud type–dependent assumptions on CWP distribution, artifacts common to the operational algorithm (which contribute to high errors) are reduced. Special accommodations are made for handling optically thin cirrus and deep convection. An application to *SNPP* VIIRS is demonstrated, and the results are compared against global *CloudSat* observations. From the VIIRS–*CloudSat* daytime matchups (September–October 2013 and January–May 2015), the new algorithm outperforms the operational *SNPP* VIIRS algorithm, particularly when the retrieved CTH is accurate. Best performance is expected for single-layer liquid-phase clouds.

1. Introduction

Clouds in the atmosphere are of fundamental importance to many theoretical and applied science topics. As clouds have significant effects on radiative, chemical, and thermodynamic feedback processes, information on the complete vertical distribution structure of clouds is

necessary to improve weather and climate models (Slingo and Slingo 1988; Randall 1989). Such information may be also used as input to generate satellite operational products, such as cloud cover fraction and cover layer retrievals (e.g., low–mid–high cloud layer information), that are used by National Weather Service (NWS) forecasters. Vertical cloud distributions, and particularly cloud-base height (mostly referred to as "cloud ceiling" when referring to the cloud layer closest to the surface), is a key parameter for the aviation community (Vislocky and Fritsch 1997; Forsythe et al. 2000; Hansen 2007; Marzban et al. 2007; Miller et al. 2014). Knowledge of the cloud-base height (CBH) with respect to the freezing level is of prime importance to identify the vertical extent of potential aircraft icing hazards as well as pilot visibility (e.g., Ellrod 2002; Mecikalski et al. 2007).

Next-generation satellite sensors are well suited to characterizing many properties of global cloud. The Visible Infrared Imaging Radiometer Suite (VIIRS) on board the *Suomi–National Polar-Orbiting Partnership* (*SNPP*) mission launched on 28 October 2011 (Hillger et al. 2013), for example, is the first next-generation polar-orbiting satellite of the Joint Polar Satellite System (JPSS; Goldberg et al. 2013) series. VIIRS provides valuable atmospheric, cloud, and surface information for both weather and climate applications. The original JPSS CBH environmental data record (EDR), based on the algorithm of Hutchison (2002) and Hutchison et al. (2006), was adapted to VIIRS as a first attempt to retrieve three-dimensional cloud fields on a large scale from an operational satellite platform (Baker 2011). Validation to assess the original CBH product processed operationally by the interface data processing segment (IDPS) has been conducted using orbital matchups with *CloudSat* (Seaman et al. 2017), which carries a non-scanning 94-GHz cloud radar capable of observing multilayered cloud profiles at 250-m vertical resolution. These evaluations revealed that the IDPS CBH retrieval performs poorly for all cloud types, and standard deviations of error for the individual granules are often greater than the JPSS measurement uncertainty requirements for the VIIRS CBH product [±2 km; per specifications outlined in Baker (2011)]. Strong dependencies of the IDPS algorithm on inputs such as cloud phase and cloud type–dependent water content contribute to the uncertainties.

With insight gained from these validation efforts, we have developed a new method that improves the performance of CBH retrievals and meets JPSS specifications for this product. This study describes a statistical approach for deriving CBH (for the uppermost cloud layer) from visible and infrared satellite measurements. The approach contains similarities to the operational IDPS algorithm for CBH in terms of retrieving a cloud geometric thickness (CGT) and subtracting this value from cloud-top height (CTH), but it follows a different method to assign CGT. Namely, it enlists satellite-based active sensing data to relate measured CGT to passive sensor retrievals of cloud water path. We assess the performance of this new CBH algorithm against the operational IDPS algorithm using independent truth data from *CloudSat*. The CBH retrieval algorithm is implemented in the framework of the Clouds from Advanced Very High Resolution Radiometer (AVHRR) Extended (CLAVR-x) system with VIIRS, which is NOAA's operational cloud algorithm processing framework for the AVHRR on the NOAA Polar-orbiting Operational Environmental Satellite and is expected to be used for the NOAA Geostationary Operational Environmental Satellite–R Series (GOES-R) Advanced Baseline Imager (ABI; Walther and Heidinger 2012). The results are also evaluated within the context of CLAVR-x against *CloudSat* observations.

The paper is outlined as follows: Section 2 summarizes previous work on CBH retrievals. Section 3 describes the satellite datasets used in the construction and implementation of the CBH algorithm. Section 4 outlines the statistical CBH algorithm and quality-control measures. Section 5 presents examples of the algorithm applied to VIIRS and compares its performance against the operational IDPS results. Section 6 concludes the paper.

2. Cloud-base height retrievals

While CTH estimation from passive imaging radiometers on environmental satellites have been conducted successfully for many years (McCleese and Wilson 1976; Menzel et al. 1983; Weisz et al. 2007; Menzel et al. 2008; Heidinger and Pavolonis 2009), CBH is a much more difficult problem from these same measurements. Conventional satellite remote measurements, such infrared and visible radiance, are not able to profile clouds from top to base. Rather, they provide information about cloud-top properties and vertically integrated water content. A central challenge is relating this column-integrated quantity—the cloud water path (CWP; $g m^{-2}$)—to CGT. Empirically based assumptions on the per-volume distribution of cloud water content (CWC; $g m^{-3}$) for a given cloud type can be used to convert CWP to CGT, but the assumption that a single CWC can represent the great diversity of clouds found in nature (even among clouds of a given "type") is fraught with uncertainty.

In spite of the understood physical limitations, several studies attempted to retrieve CBH from passive satellite observations with varying levels of success. The approaches can be divided into two broadly defined categories: 1) direct

measurement extrapolation and 2) semiempirical estimation. The first approach involves relating a spatially limited subset of direct CBH measurements to other clouds in the scene through correlative techniques (e.g., Forsythe et al. 2000; Barker et al. 2011; Miller et al. 2014). The second approach utilizes a combination of retrieved cloud products and ancillary data to infer CBHs for every cloudy pixel in the satellite image (e.g., Hutchison 2002; Hutchison et al. 2006; Minnis et al. 2011; and the current work).

Initial research to retrieve CBH was focused on ground observation–based methods with limited coverage (e.g., ceilometers and radiosondes), or methods that combine satellite-based and surface-based platforms (Forsythe et al. 2000). These techniques use direct measurements of cloud base along with spatial context from passive imager data to extrapolate measurements away from their source. Specifically, spatially limited CBH observations from active sensors (radar and lidar) provide "donor" pixels that are used to estimate the CBH of cloudy pixels distributed throughout the scene ("recipients") as observed from passive imagers. Barker et al. (2011) presented a 3D construction algorithm of cloud properties from the active–passive retrieved cross-sectional information by spectral radiance matching. Sun et al. (2016) expanded this approach to estimate CBH constrained by spectral radiance matching, which assigned donor columns observed by *CloudSat/Cloud–Aerosol Lidar and Infrared Pathfinder Satellite Observations* (*CALIPSO*) to recipient pixels across MODIS imagery. Similarly, Miller et al. (2014) developed a statistical algorithm for extending a limited set of vertically resolved cloud observations (cloud-base and cloud water contents) from *CloudSat* to form 3D cloud structures from *Aqua* MODIS 2D swath measurements via cloud type–dependent statistics on decorrelation length.

Satellite retrieval–based methods have employed a variety of approaches. Wilheit and Hutchison (2000) investigated a method to estimate cloud bases of single-layer liquid clouds from a space-based combination of microwave and infrared measurements. Ellrod (2002) developed a methodology to retrieve nighttime low CBHs significant for aviation operations using two IR bands of 3.9 and 10.7 μm from the GOES imager. Chakrapani et al. (2002) derived empirical parameterizations for a few specific single-layer clouds (stratus, deep cumulus, and cirrus) by using ground observations and estimated cloud thickness from *GOES-8* cloud retrieval products. Hutchison (2002) introduced a methodology to retrieve CBHs from electro-optical imagery and applied the approach to Moderate Resolution Imaging Spectroradiometer (MODIS) data on board the National Aeronautics and Space Administration (NASA) *Terra* mission. Hutchison et al. (2006) offered a satellite-based

method for the uppermost layer base estimate with the numerous upstream cloud retrievals of CTH and other optical properties, which has been applied to *SNPP* VIIRS.

3. Data

Our approach to estimating CBH begins with globally compiled statistics between CWP and CGT by combining instantaneous passive and active sensor observations from multiple satellites of the NASA A-Train constellation (Stephens et al. 2002; L'Ecuyer and Jiang 2010), a constellation so-called for its early afternoon [1330 local time (LT) ascending node] sun-synchronous orbit. The CWP information comes from the official NASA retrievals of *Aqua* MODIS (King et al. 1997). Vertically resolved cloud geometric boundary information is derived from the combined products of *CloudSat* radar (Stephens et al. 2002) and *CALIPSO* lidar (Winker et al. 2009). The cloud profiling radar (CPR; 94-GHz nadir-looking radar) on *CloudSat* can typically penetrate all nonprecipitating clouds but has little sensitivity to optically thin cirrus and boundary layer clouds, which the *CALIPSO* Cloud–Aerosol Lidar with Orthogonal Polarization (CALIOP) lidar is able to detect well, making the two sensors complementary to reveal detailed vertical structures of clouds (Forsythe et al. 2012; Yao et al. 2013; Miller et al. 2014). The curtain of *CloudSat/CALIPSO* observations was used to obtain detailed cloud vertical structures coinciding with the CWP information from MODIS.

Several *CloudSat* standard data products provided by the *CloudSat* Data Processing Center (http://www.cloudsat.cira.colostate.edu) were used for the algorithm development and validation. Level 2B *CloudSat* geometric profile product (2B-GEOPROF-LIDAR) was used to obtain the thickness of the clouds from the *CloudSat* CPR–*CALIPSO*/CALIOP observing system and to develop relationships between CWP and CGT. The 2B-GEOPROF data (Marchand et al. 2008) offers cloud mask and radar reflectivity, which was used to assess the algorithm performance.

The *CloudSat* bus began experiencing issues with its main battery in 2011. Since then, the CPR has been configured to operate only during daylight (ascending overpasses). The *CloudSat* CPR is also sensitive to precipitation-sized hydrometeors, which when present will obscure the true CBH and introduce a low bias (lower CPR-reported CBH compared to the "true" CBH that would be defined by the cloud droplet size distribution cutoff). Because of the strong dependency of radar reflectivity on the largest hydrometeors present in the range gate, there is no effective way to determine the CBH in the presence of precipitation. To minimize

consideration of precipitating cloud profiles, precipitation flags in the *CloudSat* 2C precipitation column algorithm (2B-PRECIP-COLUMN) product are also utilized. For CWP information, MODIS Level 2 CWP values (MYD06) that overlap and surround each *CloudSat* CPR footprint are used.

The new CBH algorithm is applied to *SNPP* VIIRS. VIIRS is an optical-spectrum scanning radiometer, one of the five instruments aboard the *SNPP* satellite that is a sun-synchronous orbit satellite with an inclination of 98.7°. It crosses the equator at about 0130 LT (descending) and 1330 LT (ascending). VIIRS has 16 moderate resolution bands (M bands) with a spatial resolution of about 750 m at nadir, five imagery bands (I bands) with a resolution of about 375 m, and the day–night band (DNB) in the visible and infrared spectral range (0.4–12 μm) with a swath width of ~3000 km (Hillger et al. 2013).

4. Algorithm description

a. Statistical construct

The VIIRS CBH product described in this paper is an estimate of the height of the base of the *topmost* cloud layer above mean sea level, obtained by subtracting the derived CGT from VIIRS-retrieved CTH. The CTH and the CWP that is used in estimation of CGT come from upstream retrieval products. CBH is retrieved only for pixels that are classified as cloudy or probably cloudy by the VIIRS cloud mask.

Our CBH retrieval is predicated on the assumption that a relationship exists between CGT and column-integrated water path, and that this relationship varies with cloud location in the vertical. To first order, these assumptions are similar to those of the original IDPS CBH algorithm (Hutchison et al. 2006). The IDPS CBH algorithm uses numerous upstream cloud retrievals, such as CTH and CWP (liquid and ice), along with specific assumptions about cloud type–dependent water contents. CGT is computed via a ratio of the retrieved CWP and the cloud type–dependent water content. Cloud type is a discretely defined quantity and the association of a characteristic liquid or ice water content gives rise to large uncertainties, reflected in findings from our validation work (Seaman et al. 2017). With the insight from the validation results and statistical analyses to obtain 3D cloud structures from *CloudSat* observations shown in Miller et al. (2014), we have developed an alternative regression method to improve CBH retrievals by using directly measured CGT global statistics, stratified by CTH, and expressed as a function of CWP.

The basis of the new statistical CBH algorithm is illustrated in Fig. 1. Geometric thickness of the uppermost layer, as provided by 2B-GEOPROF-LIDAR, is plotted versus MYD06 for a set of 100 daytime orbits from July 2007. MODIS was used in this analysis because of the formation flight of *Aqua* with *CloudSat*/*CALIPSO* and for its similarity in terms of retrieved cloud optical property (e.g., King et al. 1997) information to VIIRS. Sample matchups for CTHs residing between 0 and 14 km are plotted here. Similar relationships were calculated for CTH residing in 2-km vertical bins ranging from the surface to the top of the troposphere. Owing to the lack of the MODIS CWP retrieval at night [which is reliant on cloud optical thickness (COT) and effective particle size (EPS) from the solar reflectance bands], all cases are from daytime. In the figure, CGT rapidly increases in a nearly linear fashion for CWP values between 0 and 0.2 kg m^{-2}. A flattening and broadening of scatter occurs above 0.2 kg m^{-2}, reflecting the saturation of measurements and the weaker relationship between the CWP and CGT for optically thicker clouds.

An initial two-piece linear regression was constructed for July data from 2007 to 2010, based on a total of 1743 granules (orbits) of *CloudSat*/*CALIPSO* data (59 036 profiles). The regression fits were calculated in 2-km range bins of CTH from the lowest range (0–2 km) up to 20 km as derived from the MODIS cloud-top pressure (CTP) product. Please note that these were derived with the combined lidar–radar product (2B-GEOPROF-LIDAR), so the *CALIPSO* lidar has information on bases closer to the surface, although the *CloudSat* radar has the ground clutter issue. For the purpose of determining which range bin to populate, CTP was converted to CTH via coincident temperature profiles from the ECMWF model analysis [*CloudSat* ECMWF auxiliary (ECMWF-AUX) data; see Partain 2007 for more details]. The median value of the MODIS CWP in each 2-km CTH range bin was determined, and a linear regression above and below this threshold value was performed. This approach preserves the linear response at low CWP in Fig. 1 and provides the capability for estimating cloud thickness for deeper clouds. The results based on the two-piece linear fit are summarized in Table 1.

b. Algorithm implementation in the NOAA CLAVR-x system

For the purpose of facilitating demonstrations on VIIRS (and potentially other satellite platforms), the new CBH algorithm has been implemented in the CLAVR-x processing system. A schematic diagram of the algorithm flow is shown in Fig. 2. The CBH product requires a priori information on CTH and CWP. The CWP is derived using VIIRS retrievals of COT and EPS. These algorithms are embedded in the current CLAVR-x
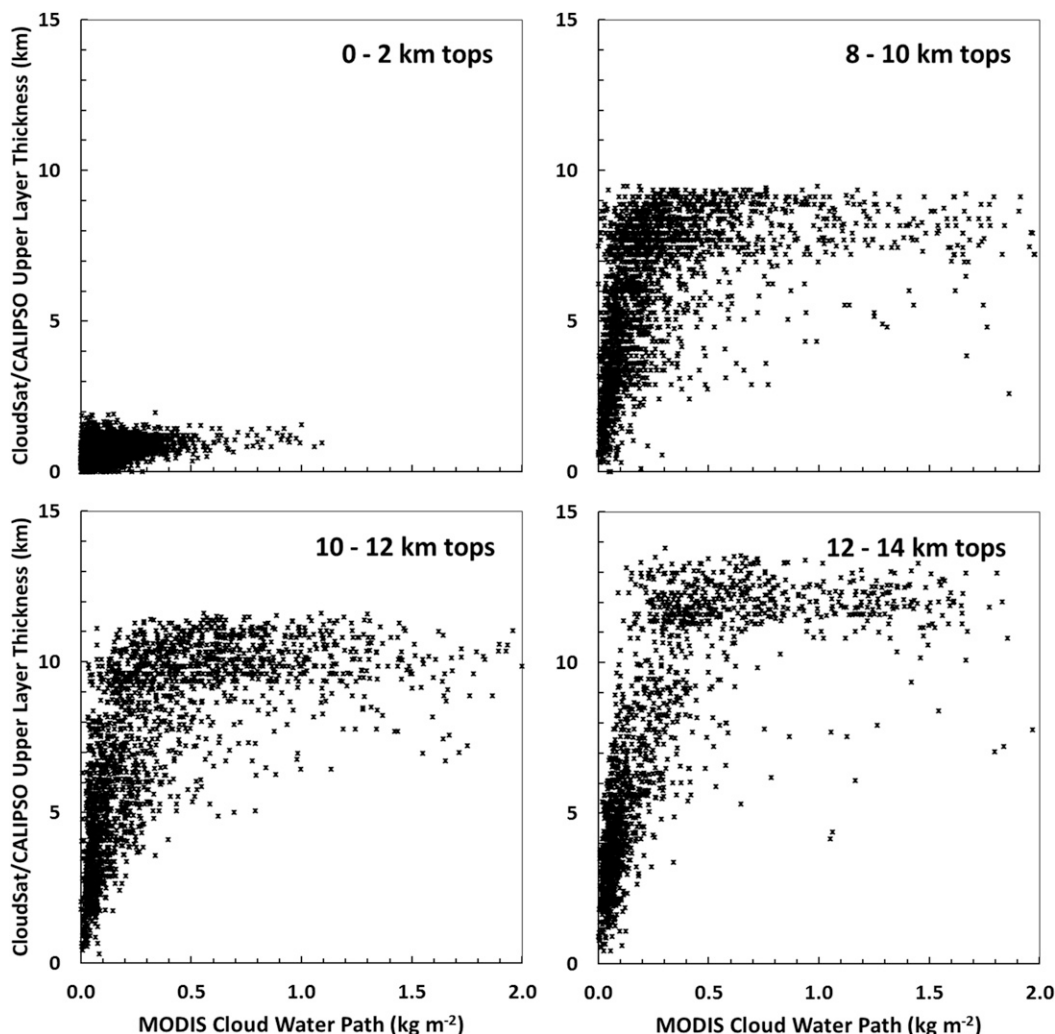
FIG. 1. MODIS cloud water path vs *CloudSat/CALIPSO* cloud geometric thickness of the uppermost layer for tops between 0 and 14 km for matchups in July 2007.

system. Currently, the daytime cloud optical and microphysical properties (DCOMP; Walther and Heidinger 2012) and nighttime lunar cloud optical and microphysical properties (NLCOMP; Walther et al. 2013) algorithms are available in the CLAVR-x system. CTH is produced from the NOAA Algorithm Working Group (AWG) cloud height algorithm (ACHA; Heidinger 2013) using IR channels, which is also part of the CLAVR-x. In rare cases when both DCOMP and NLCOMP products are not available, an IR-based cloud optical property output from ACHA is used for the CBH algorithm.

The CBH algorithm uses the CTH and CWP parameters to interrogate the height-dependent lookup table of piecewise linear coefficients (Table 1) that relates them to CGT. Once the appropriate coefficients are determined for the (CTH–CWP) pairing, CGT is computed according to

$$CGT = a \times CWP + b. \qquad (1)$$

This geometric thickness is then subtracted from the retrieved CTH to yield the final estimate of CBH:

$$CBH = CTH - CGT. \qquad (2)$$

For pixels where VIIRS is incapable of retrieving valid CWP, the corresponding NWP field values could be used as supplementary data.

c. Handling of deep convection

Very large COT (and commensurately large CWP) occurs for most deep convective clouds. Here, the CGT estimates are likely to not be as accurate as a simple estimate of cloud base predicated on the

TABLE 1. Regression coefficients and median CWPs binning by CTH (every 2 km) derived from *CloudSat*/*CALIPSO* and MODIS data (59 036 profile samples in July 2007–10), which are used to compute CGT for CBH. The slope/intercept data in the second row of each grouping apply to CWP at or above the CWP threshold shown in the second column.

CTH ranges (km)	CWP threshold ($g\,m^{-2}$)	Constant a (slope)	Constant b (y intercept)
$0 < \text{CTH} < 2$	71	2.2581	0.4056
		0.9970	0.5170
$2 \leq \text{CTH} < 4$	114	6.1098	0.6648
		0.9130	1.3570
$4 \leq \text{CTH} < 6$	110	11.5574	1.2253
		1.3792	2.5866
$6 \leq \text{CTH} < 8$	123	14.5382	1.7057
		1.6871	3.6228
$8 \leq \text{CTH} < 10$	131	9.0986	2.1425
		2.4595	3.8696
$10 \leq \text{CTH} < 12$	127	13.5772	1.8655
		4.8309	3.5314
$12 \leq \text{CTH} < 14$	115	16.0793	1.6497
		5.0517	3.9861
$14 \leq \text{CTH} < 16$	116	14.6030	2.0001
		6.0644	4.0330
$16 \leq \text{CTH}$	99	9.2658	2.2964
		6.6043	3.2644

thermodynamic factors governing convective cloud-base formation. In such cases of optically thick deep convection (defined experimentally as CWP $\geq 1000\,g\,m^{-2}$ when CTH ≤ 6.5 km, CWP $\geq 1200\,g\,m^{-2}$ when CTH ≥ 7.5 km, and linearly changing CWP thresholds in between those bounds), the CBH estimate is tied to the convective condensation level as derived from numerical weather prediction analysis data (CCL_NWP) corresponding to the cloud's location,
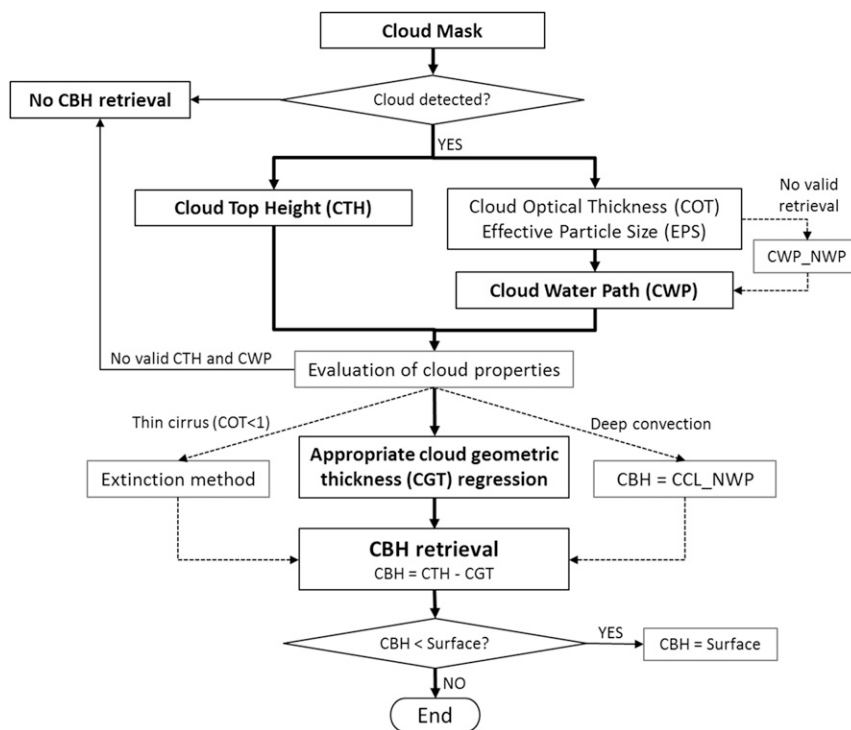

FIG. 2. A schematic diagram of the statistical CBH algorithm for the uppermost cloud layer.

$$CBH_{deep\_convection} = CCL_{\_NWP}. \qquad (3)$$

Determining the threshold for setting CBH to the NWP-derived CCL remains an area of active research. The current estimate of $1000\,g\,m^{-2}$ provides a reasonable first-order assumption that is being investigated through analysis of *CloudSat* observations of convective anvil structure with relation to precipitation shafts. The relationship of CWP to anvil depth and convective cloud base formation has, in initial work, demonstrated some variability; it is thought that different convective systems (e.g., tropical vs midlatitude) may have different CWP thresholds that could be used to more accurately determine the crossover to CCL for CBH estimates.

d. Handling of thin cirrus

A cloud extinction–based method developed by using *CALIPSO* data is employed for better CBH estimates of thin cirrus. The extinction method is an effective way of retrieving cloud base for upper-level thin cirrus cloud, and its capability has been assessed using both ground-based and space-based observations. Cirrus cloud has COT less than 2 in general, and we assume that the satellite passive-sensor-retrieved CTH is located at the vertical center of the cloud. The geometric thickness can be computed knowing COT and the extinction coefficient. The infrared-based COT retrieved in the CLAVR-x system is discussed in detail in Heidinger et al. (2015). Since cirrus is optically thin and therefore the observations are sensitive to the entire extinction profile through the cloud, it is also reasonable to assume a constant extinction coefficient.

For computing the extinction coefficients, we take advantage of *CALIPSO*/CALIOP data, which provide the vertical profiles of cloud layers and are fairly accurate in determining COT and cloud upper/lower boundaries, particularly for high thin clouds. The *CALIPSO* Level 2 5-km cloud layer product for September 2013 was used, and only single-layer clouds with COT less than 2 were chosen for the analysis. The extinction coefficients are computed as dividing CALIOP-derived CGT by COT. Table 2 shows the extinction coefficients derived for five cloud-top temperature (CTT) intervals.

For the performance test, CBH comparisons between VIIRS (using the new CBH retrieval method but without the specialized cirrus regression algorithm) and *CloudSat* were conducted using September–October 2013 quality-controlled matchups (more details in section 5). For thin cirrus clouds (COT less than 1), the results with the extinction method provided statistically better CBH estimates for thin cirrus than the original regression method; the error (bias) was improved from

TABLE 2. Mean cirrus cloud extinction coefficients for five CTT intervals.

CTT interval (K)	<200	200–220	220–240	240–260	>260
Cirrus extinction (km^{-1})	0.13	0.25	0.39	0.55	0.67

1.4 to $-0.5\,km$, the root-mean-square error (RMSE) improved from 1.9 to $1.3\,km$, the standard deviation of the errors improved from 1.3 to $1.2\,km$, and correlation coefficient r^2 increased from 0.72 to 0.78. The extinction-based method has been implemented in the current version of the CBH algorithm for better CBH estimates of thin cirrus, which are currently implemented in the CLAVR-x system. It is found out that using CTT varied coefficients show superior performances compared to a fixed value. Efforts are still ongoing for deriving better coefficients.

e. Quality control

As a quality-control filter, VIIRS pixels have been excluded when the CBH retrieval produces an out-of-range value (less than $0\,km$ or greater than $20\,km$) or has been assigned poor quality according to the granule's quality flags. It is considered that the quality flags are the integrated outcome of the upstream quality flags as well as the CBH algorithm itself. Specifically, the CBH product is a strong function of CTH and CWP (derived from COT and EPS). If these upstream input data enter the CBH algorithm with out-of-range/poor-quality flags triggered, then we assume that the CBH processing should inherit that information and not attempt a valid CBH estimate based on dubious information at that pixel.

5. Application to *SNPP* VIIRS

The CBH algorithm was applied to *SNPP* VIIRS data and the performance was assessed through comparisons with *CloudSat* measurements matched in space/time to VIIRS. The retrievals are performed for two periods: September–October 2013 and January–May 2015. We assess the accuracies of CBH and CTH using *CloudSat* data as truth, and the details for the VIIRS–*CloudSat* matchups can be found in Seaman et al. (2017). In particular, since the CTH accuracy is critical to the CBH retrieval in the algorithm, the results shown here are primarily from "Within Spec" (or quality controlled) analysis. Within Spec means only cloudy pixels where the VIIRS CTH retrieval is within $1\,km$ if the COT is greater than 1, or within $2\,km$ if the COT is less than 1 compared to *CloudSat*. In examining the comparison results, it is noted that the VIIRS system specification uncertainty requirement is $2\,km$ for CBH (Baker 2011).
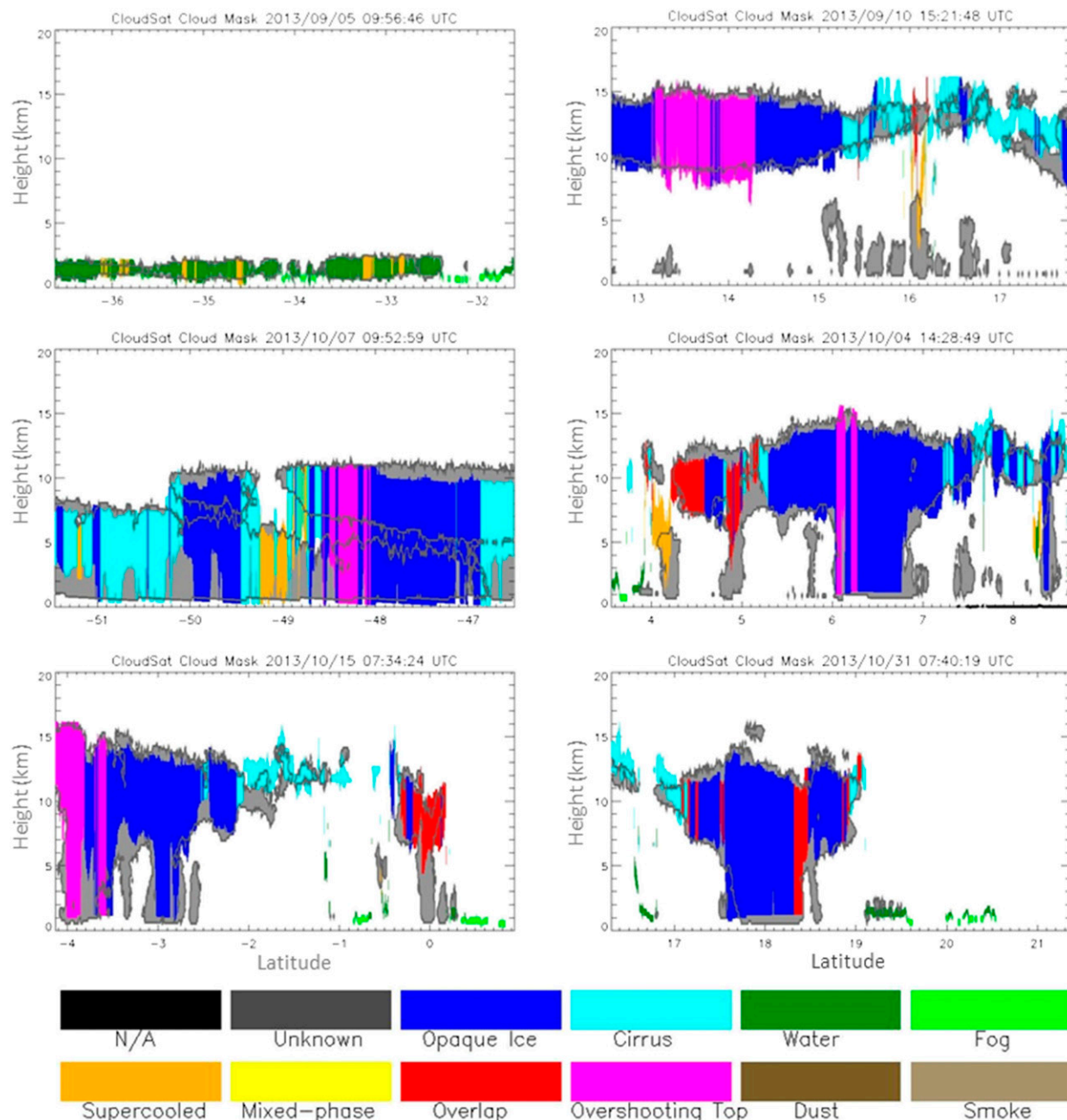
FIG. 3. CBH retrievals from the statistical CBH retrieval algorithm for selected VIIRS granules during the September–October 2013 VIIRS *CloudSat* matchup period. The *CloudSat* cloud boundaries from 2B-GEOPROF data are shown in gray, and the VIIRS CTH and CBH retrievals are colored according to cloud type (obtained from CLAVR-x with VIIRS) for comparison purposes.

a. Case studies

Figure 3 shows sample VIIRS–*CloudSat* matchups collected from the September–October 2013 cases. Clouds detected by *CloudSat* are shaded in gray. The VIIRS-retrieved CTHs and CBHs are colored by VIIRS-defined cloud type over each matchup *CloudSat* profile. In general, when CTH retrievals are accurate,

the statistical CBH retrievals are seen to show good agreement with *CloudSat* for all cloud types. However, as shown in the middle-left panel of Fig. 3, there is a possibility that *CloudSat* observes multiple cloud layers, such as cirrus over a thick low-level cloud, and CBH is placed at the lower layer (or between the layers) due to assigning the entire CGT to the upper layer by high CWP retrieval. The algorithm will retrieve primarily the
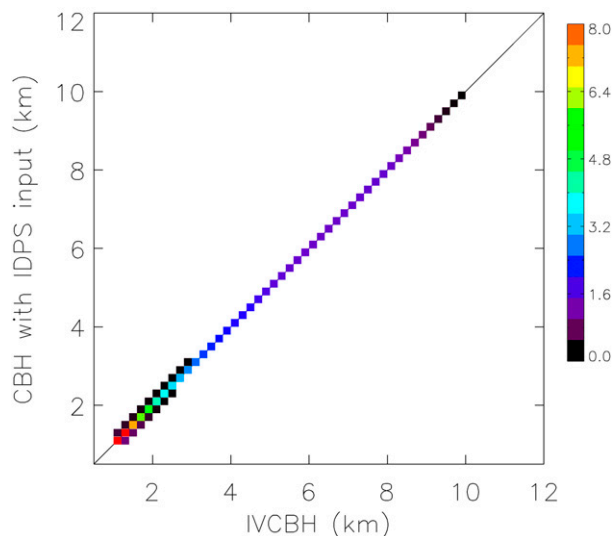
FIG. 4. Sample histogram of CBH comparisons from the operational IDPS CBH product (IVCBH) vs the reconstructed stand-alone code based on the IDPS CBH algorithm for 113 VIIRS granules in September 2013 (in percentages of the total pixel number).

b. Comparisons against the operational algorithm

We have analyzed the performance of the current algorithm vis-à-vis the original VIIRS IDPS CBH algorithm. Since any errors specific to the upstream IDPS cloud products would propagate into CBH, introducing ambiguity when comparing against the new algorithm that uses CLAVR-x cloud products, we implemented a stand-alone code of the IDPS CBH algorithm as based on the original JPSS VIIRS CBH algorithm theoretical basis document (ATBD) of Baker (2011) and utilized the CLAVR-x-supplied ancillary cloud property input data to provide a proxy to keep consistency in the comparison. The performance of this code has been verified against the IDPS CBH algorithm as shown in Fig. 4. The figure shows the CBHs from the stand-alone code with the IDPS upstream are consistent with the operational IDPS CBH product [Intermediate VIIRS CBH product (IVCBH)].

For these comparisons, estimates in the lowest 1 km (above ground level), where ground clutter contaminates the *CloudSat* CPR data (Marchand et al. 2008), were excluded from the analysis. We also removed any precipitation-contaminated (as identified by nonzero *CloudSat* column precipitation retrievals) and error-filled data. A total of 1 051 243 matchup profiles taken from 2077 VIIRS granules were considered. After the quality-controlled filters were applied, 95 145 Within Spec (with regard to VIIRS agreement with active sensor CTH data) matchup points remained for use in our validation.

Figures 5 shows histograms of the original IDPS algorithm (stand-alone code, with cloud and data supplied

cloud base of the uppermost layer cloud if lower clouds are not well detected and the column-integrated CWP retrieval is made for the topmost layer, which shows that the accuracy and representativeness of the upstream CWP retrieval is essential to the CBH estimate together with the CTH accuracy. It should be noted that multi-layer cloud scenes are typically more challenging for CTH and CBH retrievals, and CLAVR-x CTH also often tends to be biased low for the multilayer situation.
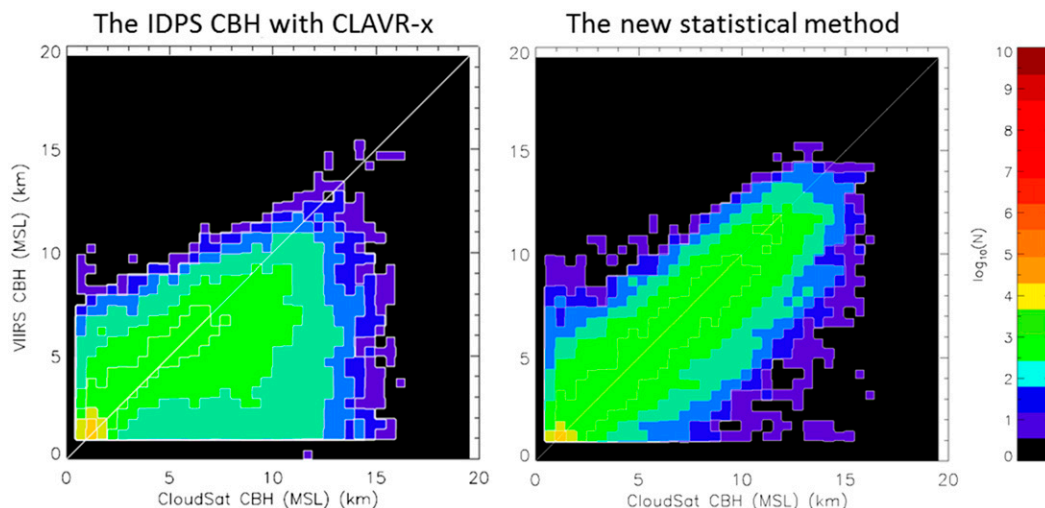

FIG. 5. (left) Quality-controlled two-dimensional histograms of VIIRS-retrieved and *CloudSat*-observed CBH for the original IDPS CBH algorithm with CLAVR-x input, and (right) the statistical algorithm (implemented in the CLAVR-x system) for September–October 2013. Colors represent the number of data points (*N*; shown on a logarithmic scale). The comparisons are valid for all cloud types encountered globally.
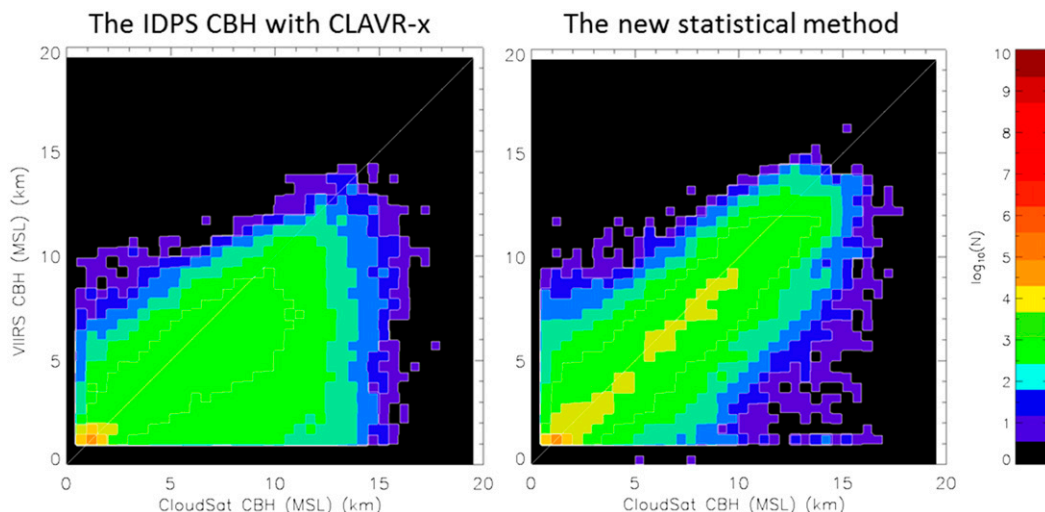
FIG. 6. As in Fig. 5, but for January–May 2015.

by CLAVR-x) and the new CBH algorithm using *CloudSat* as "truth" data for CBH, compiled for September–October 2013 VIIRS–*CloudSat* orbital matchups. Initial results show the current statistical regression method outperforms the original IDPS CBH algorithm with CLAVR-x upstream input, with a tighter clustering of points along the 1:1 agreement line (Fig. 5). The validation period was extended to the January–May 2015 matchups, with results shown in Fig. 6. Here, a total of 2 718 982 matchup profiles from 5358 VIIRS granules were examined, and 216 745 Within Spec points survived quality control. The general performance pattern is very similar to the September–October 2013 matchups.

Analyzing the performance of the new CBH algorithm for both matchup periods, we deduced that the outlier points having high *CloudSat*-observed CBH (>10 km) but very low VIIRS-reported CBH occurred for cases when *CloudSat* identified a thin upper cloud layer that was not detected or misrepresented by VIIRS. Multilayered cloud systems, where the column-integrated CWP factors into producing larger CGT, can also lead

to low biases in VIIRS-derived CBH in comparison to the CBH of the uppermost cloud layer seen by *CloudSat*. Another source of bias, where VIIRS-derived CBH is high but *CloudSat*-observed CBH extends almost to the surface, could be due to lingering precipitation-contaminated *CloudSat* data. Although we are using precipitation flags from 2C-PRECIP-COLUMN to filter out those profiles in the comparisons, some unfiltered profiles may remain. Further research is ongoing for the algorithm refinement.

Various statistical analyses were conducted to quantitatively investigate CBH algorithm performance for the selected matchup periods. Tables 3 and 4 summarize CBH error statistics (using *CloudSat* as truth) for all clouds (values in boldface) and each cloud type for September–October 2013 matchups (Table 3) and January–May 2015 matchups (Table 4) for quality-controlled data. Statistics (error magnitudes) derived from *CloudSat* on CGTs as a function of VIIRS cloud type was shown to examine skill with respect to conventional climatology purposes, even though the

TABLE 3. Error statistics of CBHs for the new algorithm, taken from VIIRS–*CloudSat* matchups for September–October 2013 (95 145 quality-controlled matchup points).

CBH (km) Within Spec only	Samples (%)	Avg error (bias)	Std dev of error	Median error	RMSE	r^2	CBH within 250 m of *CloudSat* (%)
All	**100**	**0.3**	**1.7**	**0.2**	**1.7**	**0.791**	**19.9**
Cirrus	51	0.3	1.7	0.2	1.7	0.698	12.6
(thin)	(6)	(−0.5)	(1.2)	(−0.5)	(1.3)	(0.775)	(15.4)
Opaque ice	14	0.3	2.3	0.1	2.3	0.515	11.4
Water	9	0.2	0.5	0.2	0.5	0.688	53.6
Supercooled	21	0.3	1.1	0.1	1.1	0.688	30.5
Overlap	4	0.4	2.1	0.3	2.1	0.502	10.6
Overshooting	1	0.8	2.8	0.6	3.0	0.295	9.1

TABLE 4. As in Table 3, but for January–May 2015 (216 745 quality-controlled matchup points).

CBH (km) Within Spec only	Samples (%)	Avg error (bias)	Std dev of error	Median error	RMSE	r^2	CBH within 250 m of *CloudSat* (%)
All	**100**	**0.4**	**1.6**	**0.3**	**1.7**	**0.803**	**19.8**
Cirrus	49	0.5	1.7	0.3	1.7	0.729	12.2
(thin)	(5)	(−0.4)	(1.3)	(−0.4)	(1.3)	(0.770)	(14.7)
Opaque ice	12	0.5	2.3	0.3	2.3	0.486	11.3
Water	10	0.2	0.5	0.1	0.6	0.770	51.2
Supercooled	23	0.4	1.1	0.2	1.2	0.671	29.2
Overlap	5	0.4	2.2	0.3	2.2	0.447	10.8
Overshooting	1	0.6	3.4	0.2	3.5	0.196	7.5

algorithm as currently designed is not cloud type dependent (with the exception of thin cirrus). A few minor types with negligible samples were not included in the tables. The values for thin cirrus where the extinction-based method has been adopted are shown in parentheses. In the tables, matchup points where the error is less than 250 m (the vertical resolution of *CloudSat*) are considered to be accurate. In general, the new CBH algorithm shows good agreement with *CloudSat* so long as the CTH accuracy requirement is satisfied. Moreover, the performance of the new algorithm satisfies the JPSS measurement uncertainty requirements for the VIIRS CBH EDR product (±2 km). The performance is best for water clouds and leaves room for further improvement in cases of overlapping (multilayered) and tropopause-overshooting cloud systems as well as opaque ice clouds (e.g., thick anvil cirrus that may have sufficiently high CWP to trigger our NWP-based CCL estimate, incurring large errors in the process). We take care to point out via Tables 3 and 4 that the percentages of opaque ice and overshooting-top cloud types are relatively low compared to the majority of clouds encountered in our validation cases. For comparison purposes, similar error statistics are summarized in Tables 5 and 6 for CBHs (values in boldface for all clouds) from the IDPS algorithm shown in Figs. 5 and 6, respectively. It is supposed that the decreased numbers of CBHs from the IDPS algorithm are due to errors of upstream inputs

related to determining cloud type or cloud phase. From the results, we can see the new CBH algorithm outperform the IDPS algorithm for all clouds. The IDPS algorithm shows similar performance only for water clouds.

6. Conclusions

A statistical regression algorithm for estimating CGT and CBH of the uppermost cloud layer has been developed and evaluated using multisensor observations from the NASA A-Train constellation. It has been integrated into the NOAA CLAVR-x framework and is now being implemented in the NOAA JPSS operational cloud product system. The CGT is predicated on the relationships drawn between observed CGT (from *CloudSat/CALIPSO*) and CWP (from *Aqua* MODIS), conditioned on CTH. The CBH is then calculated by subtracting the derived CGT from a retrieved value of CTH. The regression coefficients used for the piecewise linear fit that relates CGT to CWP were computed to form an a priori lookup table.

The most critical upstream inputs for the CBH retrieval are the CTH and CWP (which is derived from COT and EPS). In addition, the accuracy of the CBH is proportional to that of CTH. Thus, the errors in CTH and CWP are added to the CBH retrieval output. The new statistical approach avoids errors arising from incorrect cloud type and phase assignment. We have made

TABLE 5. As in Table 3, but for the IDPS CBHs shown in Fig. 5 (85 495 quality-controlled matchup points for September–October 2013 matchups).

CBH (km) Within Spec only	Samples (%)	Avg error (bias)	Std dev of error	Median error	RMSE	r^2	CBH within 250 m of *CloudSat* (%)
All	**100**	**0.7**	**2.6**	**−0.1**	**2.7**	**0.452**	**18.0**
Cirrus	37	1.9	3.0	1.3	3.5	0.111	8.4
Opaque ice	8	3.1	2.8	2.7	4.2	0.147	4.7
Water	17	−0.2	0.5	−0.2	0.6	0.747	50.2
Supercooled	33	−1.1	1.1	−0.8	1.6	0.719	15.4
Overlap	4	1.5	2.5	1.2	2.9	0.234	9.0
Overshooting	0.3	3.2	3.0	3.2	4.4	0.106	3.9

TABLE 6. As in Table 4, but for the IDPS CBHs shown in Fig. 6 (162 079 quality-controlled matchup points for January–May 2015).

CBH (km) Within Spec only	Samples (%)	Avg error (bias)	Std dev of error	Median error	RMSE	r^2	CBH within 250 m of CloudSat (%)
All	**100**	**1.3**	**2.6**	**0.5**	**2.9**	**0.489**	**19.3**
Cirrus	47	2.0	3.0	1.4	3.6	0.145	7.8
Opaque ice	10	3.1	2.7	2.8	4.2	0.176	4.0
Water	22	−0.2	0.5	−0.2	0.5	0.755	50.8
Supercooled	12	0.6	1.6	0.4	1.7	0.475	16.3
Overlap	5	1.4	2.6	1.2	2.9	0.212	8.4
Overshooting	0.4	3.1	3.2	2.9	4.5	0.166	4.5

special provisions for particularly challenging cloud types, applying extinction-based method for cirrus (COT < 1) to estimate better CBH retrievals and enlisting NWP data to assign CCL_NWP as the CBH for deep convection.

Given the understood physical limitations of any passive-based approach to retrieving CBH, initial results for the new algorithm as applied to *SNPP* VIIRS and validated using *CloudSat* are very encouraging. The new CBH algorithm overall works well, optimally for single-layered liquid-phase clouds and when CTH is in close agreement with *CloudSat*. In particular, these comparisons show that the statistical retrieval approach outperforms the operational IDPS algorithm for all cloud types. The IDPS algorithm shows similar performance only for water clouds. It should be noted *CloudSat* CPR has relatively less sensitivity to optically thin clouds and has a tendency to underestimate VIIRS CTH, compared to *CALIPSO*. Further efforts to combine the information from both sensors are ongoing for more detailed validation, which became challenging due to the difficulty in maintaining tight formation flying of two satellites since the *CloudSat* battery anomaly occurred in April 2011 (Nayak et al. 2012).

Many problems remain to be solved to produce a feasible algorithm for more complex cloud systems. The retrieved CBH does not always correspond to what is considered a "ceiling" in the aviation community. Multilayered clouds (in cases where there is sufficient optical and thermal separation) are possibly identified as an output from the CLAVR-x system (Pavolonis and Heidinger 2004), but the current CBH algorithm is predicated on a single-layer cloud. Thus, there could be a lower cloud layer below our retrieval base.

CBH is currently retrieved for both daytime and nighttime as long as valid CTH and CWP values exist, although the regression method has been developed with daytime satellite data. Analyses with ground observations for nighttime performance are currently in progress. These could not be accomplished with *CloudSat* (no nighttime data due to a battery issue) in

the VIIRS era. Algorithm performance might be degraded at night depending on the CWP accuracy from the nighttime cloud optical property retrievals.

Efforts to further improve the current CBH algorithm are ongoing. We plan to stratify the regression statistics by land and ocean as a way of accounting for continental versus maritime airmass dependencies on cloud microphysics and morphology. We are working toward higher-order piecewise fits to the CGT versus CWP for the various CTH stratifications. While special handling of cirrus and deep convection has already yielded statistical performance improvements, we also plan to examine adiabatic modeling of cloud water distribution for low marine clouds (e.g., Bennartz 2007).

Building on this work, the statistical CBH estimation method will be used to improve the VIIRS cloud cover and layers (CCL) EDR, which reports fractional cloud cover for various prescribed tropospheric layers. The new version of CCL will approximate the cloud amount of middle/lower layers, more accurately incorporating CGT, which spans the column, as opposed to using a single value of CTH and no further information on cloud vertical extent. This retrieval technique, demonstrated here with VIIRS, can be applied to other sensors that are able to retrieve CTH and CWP. The *Himawari-8/9* Advanced Himawari Imager, the GOES-R Advanced Baseline Imager, and a host of other next-generation geostationary sensors have the capacity to work with this algorithm. Implementation of the algorithm on these geostationary systems will increase opportunities for calibration/validation of the algorithm against active sensors flying on low-Earth-orbiting satellites.

REFERENCES

Baker, N., 2011: Joint Polar Satellite System (JPSS) VIIRS cloud base height algorithm theoretical basis document (ATBD). JPSS Ground Project Code 474-00045, NASA GSFC, 35 pp. [Available online at http://www.star.nesdis.noaa.gov/jpss/documents/ATBD/D0001-M01-S01-015_JPSS_ATBD_VIIRS-Cloud-Base-Height.pdf.]

Barker, H. W., M. P. Jerg, T. Wehr, S. Kato, D. P. Donovan, and R. J. Hogan, 2011: A 3D cloud-construction algorithm for the EarthCARE satellite mission. *Quart. J. Roy. Meteor. Soc.*, **137**, 1042–1058, doi:10.1002/qj.824.

Bennartz, R., 2007: Global assessment of marine boundary layer cloud droplet number concentration from satellite. *J. Geophys. Res.*, **112**, D02201, doi:10.1029/2006JD007547.

Chakrapani, V., D. R. Doelling, A. D. Rapp, and P. Minnis, 2002: Cloud thickness estimation from GOES-8 satellite data over the ARM-SGP site. *Proc. 12th ARM Science Meeting*, St. Petersburg, FL, U.S. Dept. of Energy, 7 pp.

Ellrod, G. P., 2002: Estimation of low cloud base heights at night from satellite infrared and surface temperature data. *Natl. Wea. Dig.*, **26** (1–2), 39–44.

Forsythe, J. M., T. H. Vonder Haar, and D. L. Reinke, 2000: Cloud-base height estimates using a combination of meteorological satellite imagery and surface reports. *J. Appl. Meteor.*, **39**, 2336–2347, doi:10.1175/1520-0450(2000)039<2336:CBHEUA>2.0.CO;2.

——, J. B. Dodson, P. T. Partain, S. Q. Kidder, and T. H. Vonder Haar, 2012: How total precipitable water vapor anomalies relate to cloud vertical structure. *J. Hydrometeor.*, **13**, 709–721, doi:10.1175/JHM-D-11-049.1.

Goldberg, M. D., H. Kilcoyne, H. Cikanek, and A. Metha, 2013: Joint Polar Satellite System: The United States next generation civilian polar-orbiting environmental satellite system. *J. Geophys. Res. Atmos.*, **118**, 13 463–13 475, doi:10.1002/2013JD020389.

Hansen, B., 2007: A fuzzy logic–based analog forecasting system for ceiling and visibility. *Wea. Forecasting*, **22**, 1319–1330, doi:10.1175/2007WAF2006017.1.

Heidinger, A. K., 2013: ABI cloud height. Version 3.0, NOAA/NESDIS/STAR Algorithm Theoretical Basis Doc., 79 pp. [Available online at http://www.star.nesdis.noaa.gov/goesr/docs/ATBD/Cloud_Height.pdf.]

——, and M. J. Pavolonis, 2009: Gazing at cirrus clouds for 25 years through a split window. Part I: Methodology. *J. Appl. Meteor. Climatol.*, **48**, 1100–1116, doi:10.1175/2008JAMC1882.1.

——, Y. Li, B. A. Baum, R. E. Holz, S. Platnick, and P. Yang, 2015: Retrieval of cirrus cloud optical depth under day and night conditions from MODIS Collection 6 cloud property data. *Remote Sens.*, **7**, 7257–7271, doi:10.3390/rs70607257.

Hillger, D., and Coauthors, 2013: First-light imagery from Suomi NPP VIIRS. *Bull. Amer. Meteor. Soc.*, **94**, 1019–1029, doi:10.1175/BAMS-D-12-00097.1.

Hutchison, K. D., 2002: The retrieval of cloud base heights from MODIS and three-dimensional cloud fields from NASA's EOS Aqua mission. *Int. J. Remote Sens.*, **23**, 5249–5265, doi:10.1080/01431160110117391.

——, E. Wong, and S. C. Ou, 2006: Cloud base height retrieval during nighttime conditions with MODIS data. *Int. J. Remote Sens.*, **27**, 2847–2862, doi:10.1080/01431160500296800.

King, M. D., S.-C. Tsay, S. E. Platnick, M. Wang, and K. N. Liou, 1997: Cloud retrieval algorithms for MODIS: Optical thickness, effective particle radius, and thermodynamic phase. Version 5, MODIS Algorithm Theoretical Basis Doc. ATBD-MOD-05, 79 pp.

L'Ecuyer, T. S., and J. H. Jiang, 2010: Touring the atmosphere aboard the A-Train. *Phys. Today*, **63**, 36, doi:10.1063/1.3463626.

Marchand, R., G. G. Mace, T. Ackerman, and G. Stephens, 2008: Hydrometeor detection using Cloudsat—An Earth-orbiting 94-GHz cloud radar. *J. Atmos. Oceanic Technol.*, **25**, 519–533, doi: 10.1175/2007JTECHA1006.1.

Marzban, C., S. Leyton, and B. Colman, 2007: Ceiling and visibility forecasts via neural networks. *Wea. Forecasting*, **22**, 466–479, doi:10.1175/WAF994.1.

McCleese, D. J., and L. W. Wilson, 1976: Cloud top height from temperature sounding instruments. *Quart. J. Roy. Meteor. Soc.*, **102**, 781–790, doi:10.1002/qj.49710243408.

Mecikalski, J. R., and Coauthors, 2007: Aviation applications for satellite-based observations of cloud properties, convection initiation, in-flight icing, turbulence, and volcanic ash. *Bull. Amer. Meteor. Soc.*, **88**, 1589–1607, doi:10.1175/BAMS-88-10-1589.

Menzel, W. P., W. L. Smith, and T. R. Stewart, 1983: Improved cloud motion wind vector and altitude assignment using VAS. *J. Appl. Meteor. Climatol.*, **22**, 377–384, doi:10.1175/1520-0450(1983)022<0377:ICMWVA>2.0.CO;2.

——, and Coauthors, 2008: MODIS global cloud-top pressure and amount estimation: Algorithm description and results. *J. Appl. Meteor. Climatol.*, **47**, 1175–1198, doi:10.1175/2007JAMC1705.1.

Miller, S. D., and Coauthors, 2014: Estimating three-dimensional cloud structure via statistically blended satellite observations. *J. Appl. Meteor. Climatol.*, **53**, 437–455, doi:10.1175/JAMC-D-13-070.1.

Minnis, P., and Coauthors, 2011: CERES Edition-2 cloud property retrievals using TRMM VIRS and Terra and Aqua MODIS data—Part I: Algorithms. *IEEE Trans. Geosci. Remote Sens.*, **49**, 4374–4400, doi:10.1109/TGRS.2011.2144601.

Nayak, M., M. Witkowski, D. Vane, T. Livermore, and M. Rokey, 2012: CloudSat anomaly recovery and operational lessons learned. *Proc. 12th Int. Conf. on Space Operations (Space Ops 2012)*, Stockholm, Sweden, CNES, 1295798. [Available online at www.spaceops2012.org/proceedings/documents/id1295798-Paper-001.pdf.]

Partain, P., 2007: Cloudsat ECMWF-AUX auxiliary data process description and interface control document. CloudSat Project, CIRA, Colorado State University, 11 pp. [Available online at http://www.cloudsat.cira.colostate.edu/sites/default/files/products/files/ECMWF-AUX_PDICD.P_R04.20070718.pdf.]

Pavolonis, M. J., and A. K. Heidinger, 2004: Daytime cloud overlap detection from AVHRR and VIIRS. *J. Appl. Meteor.*, **43**, 762–778, doi:10.1175/2099.1.

Randall, D. A., 1989: Cloud parameterization for climate models: Status and prospects. *Atmos. Res.*, **23**, 345–362, doi:10.1016/0169-8095(89)90025-2.

Seaman, C. J., Y.-J. Noh, S. D. Miller, A. K. Heidinger, and D. T. Lindsey, 2017: Cloud-base height estimation from VIIRS. Part I: Operational algorithm validation against *CloudSat*. *J. Atmos. Oceanic Technol.*, **34**, 567–583, doi:10.1175/JTECH-D-16-0109.1.

Slingo, A., and J. M. Slingo, 1988: The response of a general circulation model to cloud longwave forcing. I: Introduction and initial experiments. *Quart. J. Roy. Meteor. Soc.*, **114**, 1027–1062, doi:10.1002/qj.49711448209.

Stephens, G. L., and Coauthors, 2002: The CloudSat mission and the A-Train: A new dimension of space-based observations of clouds and precipitation. *Bull. Amer. Meteor. Soc.*, **83**, 1771–1790, doi:10.1175/BAMS-83-12-1771.

Sun, X. J., H. R. Li, H. W. Barker, R. W. Zhang, Y. B. Zhou, and L. Liu, 2016: Satellite-based estimation of cloud-base heights

using constrained spectral radiance matching. *Quart. J. Roy. Meteor. Soc.*, **142**, 224–232, doi:10.1002/qj.2647.

Vislocky, R. L., and J. M. Fritsch, 1997: An automated, observations-based system for short-term prediction of ceiling and visibility. *Wea. Forecasting*, **12**, 31–43, doi:10.1175/1520-0434(1997)012<0031: AAOBSF>2.0.CO;2.

Walther, A., and A. K. Heidinger, 2012: Implementation of the daytime cloud optical and microphysical properties algorithm (DCOMP) in PATMOS-x. *J. Appl. Meteor. Climatol.*, **51**, 1371–1390, doi:10.1175/JAMC-D-11-0108.1.

——, ——, and S. Miller, 2013: The expected performance of cloud optical and microphysical properties derived from Suomi NPP VIIRS day/night band lunar reflectance. *J. Geophys. Res. Atmos.*, **118**, 13 230–13 240, doi:10.1002/2013JD020478.

Weisz, E., J. Li, J. Li, D. K. Zhou, H.-L. Huang, M. D. Goldberg, and P. Yang, 2007: Cloudy sounding and cloud-top height retrieval from AIRS alone single field-of-view radiance measurements. *Geophys. Res. Lett.*, **34**, L12802, doi:10.1029/2007GL030219.

Wilheit, T. T., and K. D. Hutchison, 2000: Retrieval of cloud base heights from passive microwave and cloud top temperature data. *IEEE Trans. Geosci. Remote Sens.*, **38**, 1253–1259, doi:10.1109/36.843017.

Winker, D. M., M. A. Vaughan, A. H. Omar, Y. Hu, K. A. Powell, Z. Liu, W. H. Hunt, and S. A. Young, 2009: Overview of the CALIPSO mission and CALIOP data processing algorithms. *J. Atmos. Oceanic Technol.*, **26**, 2310–2323, doi:10.1175/2009JTECHA1281.1.

Yao, Z., J. Li, E. Weisz, A. Heidinger, and C. Liu, 2013: Evaluation of single field-of-view cloud top height retrievals from hyperspectral infrared sounder radiances with CloudSat and CALIPSO measurements. *J. Geophys. Res. Atmos.*, **118**, 9182–9190, doi:10.1002/jgrd.50681.